Cell. Mol. Life Sci. (2011) 68:1623–1631
DOI 10.1007/s00018-010-0556-7

Cellular and Molecular Life Sciences

RESEARCH ARTICLE

The crystalline phase of cellulose changes under developmental control in a marine chordate

Keisuke Nakashima · Atsuo Nishino · Yoshiki Horikawa · Euichi Hirose · Junji Sugiyama · Nori Satoh

Received: 23 April 2010 / Revised: 4 October 2010 / Accepted: 4 October 2010 / Published online: 24 October 2010

Abstract The native form of cellulose is a fibrillar composite of two crystalline phases, the triclinic I_α and monoclinic I_β allomorphs. Allomorph ratios are species-specific, and this gives rise to natural structural variations in cellulose crystals. However, the mechanisms contributing to crystal formation remain unknown. We show that the two crystalline phases of cellulose are tailored to distinct structures during different developmental stages of the tunicate chordate *Oikopleura dioica*. Larval cellulose consisting of I_α allomorph constitutes the body cuticle fin, whereas adult cellulose consisting of I_β allomorph frames a mucous filter-feeding device, the "house." Both structures are secreted from the epidermis in accordance with the mutually exclusive expression patterns of two distinct putative cellulose synthase genes. We discuss a possible linkage between structural variations of the crystalline phases of cellulose and the underlying evolutionary genetics of cellulose biosynthesis.

Keywords Cellulose · Allomorph · Tunicate · Appendicularian · *Oikopleura dioica*

Electronic supplementary material The online version of this article (doi:10.1007/s00018-010-0556-7) contains supplementary material, which is available to authorized users.

K. Nakashima (✉) · N. Satoh
Marine Genomics Unit, Okinawa Institute of Science and Technology Promotion Corporation, 1919-1 Tancha, Onna-son, Kunigami-gun, Okinawa 904-0412, Japan
e-mail: keisuke@oist.jp

K. Nakashima
Department of Zoology, Graduate School of Science, Kyoto University, Sakyo-ku, Kyoto 606-8502, Japan

A. Nishino
Department of Biological Sciences, Graduate School of Science, Osaka University, 1-1 Machikaneyama, Toyonaka 560-0043, Japan

Y. Horikawa · J. Sugiyama
Research Institute for Sustainable Humanosphere, Kyoto University, Uji, Kyoto 611-0011, Japan

E. Hirose
Department of Chemistry, Biology and Marine Science, Faculty of Science, University of the Ryukyus, Nishihara, Okinawa 903-0213, Japan

Introduction

Appendicularians are abundant pelagic tunicates, and they employ a unique filter-feeding mechanism that contributes to the oceanic carbon cycle. They live in a spherical mucous structure, termed the "house," that consists of several chambers, vessels, and filters through which their undulating tails pump sea water for filtration, enabling the efficient uptake of a wide range of organic matter as small as colloidal particles (Fig. 1a–d, Video S1) [1]. This bypasses the energy-consuming lower trophic levels in the marine food web, allowing greater energy extraction [2]. Houses are sequentially rebuilt over the lifetime of the organism, and the lifelong carbon investment can be up to 3.6 times greater than the body biomass [3]. Additionally, discarded houses contribute to the vertical ocean carbon flux, and they are the main component of marine snow [4].

Because of the unique structure and function of houses, it has long been thought that no counterparts exist among other tunicates including ascidians [5]. The body plan of adult appendicularians is also unique among tunicates; most tunicates lose the tail during the tadpole larva to adult metamorphosis, but the tail is retained by

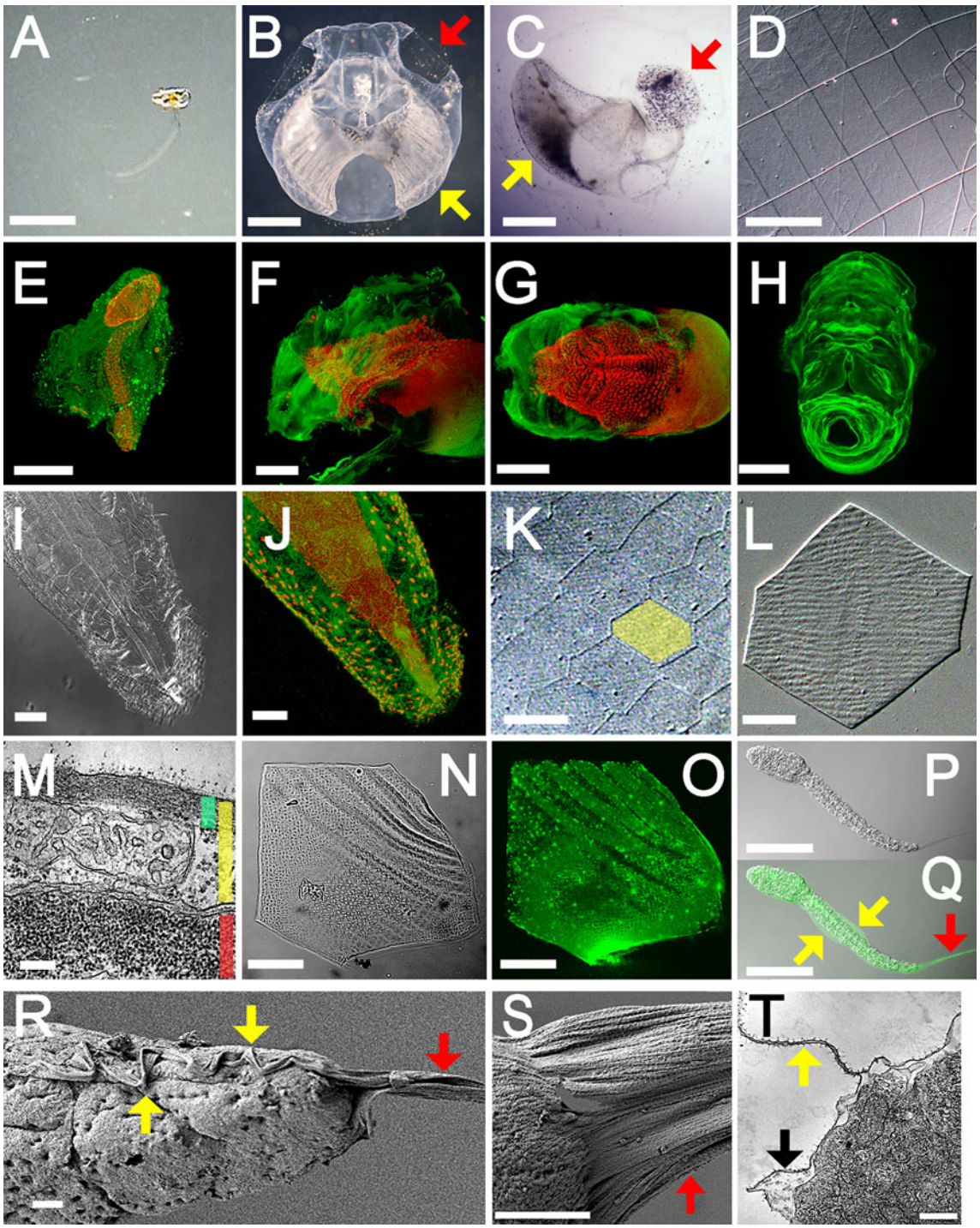

appendicularians during their biphasic life cycle [6]. Because the tail is a prerequisite for the generation of functional houses, tailless tunicates could neither construct nor maintain houses. Tunicates are so named because of the presence of a protective coat surrounding their epidermis, the tunic, which is constructed out of a unique form of animal cellulose, and houses are also made of a form of cellulose [7]. It is possible that tunics and houses may arise from a corresponding part of the progenitor, consistent with the theory of descent with modification [8]. To test this hypothesis, we examined cellulosic structures during the development of the oikopleurid appendicularians *Oikopleura longicauda* and *Oikopleura dioica*.

◀ **Fig. 1a–t** Possible cellulosic structures of *Oikopleura*. **a**–**h** House. The filter-feeding house structure is difficult to detect in its natural state (**a**, *lateral view*). Incubation of organisms with carbon particles allows the visualization of the overall internal structures (**b**, *upper view*) or filtrate meshes (**c**, *lateral view*) only (*red arrow* inlet filter; *yellow arrow* food-concentrating filter). **d** A magnified view of the inlet filter shows the regular arrangements of rectangular pores (DIC). **e** The house is visualized by CBM labeling (*green*) using confocal microscopy; nuclei are stained with TO-PRO-3 (*red*). **f**, **g** The rudimentary house before inflation, or house rudiment, is secreted from the anterior trunk epidermis (**f** *lateral view*; **g** *dorsal view*). **h** The isolated house rudiment is shown (*upper-frontal view*). **i**–**o** Scale-like structure. **i**, **j** Hexagonal flat cells of the tail epidermis are shown (**i** DIC; **j** CBM labeling). **k** The exoskeleton-like capsule consists of hexagonal scale-like structures (featured in *yellow*, DIC). **l** A single scale-like structure is shown (DIC). **m** The tail is shown in cross-section by electron micrograph; scale-like structures show intracellular localization (*green bar* scale-like structure, *yellow bar* epidermal cell, *red bar* muscle cell). **n**, **o** There is a meshwork within the scale-like structures (**n** DIC; **o** CBM labeling). **p**–**t** Larval body cuticle. **p**, **q** The larval body cuticle forms the median fins (*yellow arrow*) and a caudal fin (*red arrow*) (**p** DIC; **q** CBM labeling). **r**, **s** Scanning electron micrographs of the larval tail show the median fins (*yellow arrow*) contiguous with a caudal fin (*red arrow*). Note that many fibrils are aligned anteroposteriorly. **t** The larval tail is shown in cross-section by electron micrograph (*yellow arrow* median fin, *black arrow* larval body cuticle). *Bar* 1 mm (**a**–**c**), 100 μm (**d**, **f**–**h**, **p**, **q**), 500 μm (**e**), 20 μm (**i**–**k**), 5 μm (**l**, **n**, **o**), 200 nm (**m**, **t**), and 2 μm (**r**, **s**). **a**–**e**, **i**–**o**, **r**–**t**: *Oikopleura dioica*; **f**–**h**, **p**, **q**: *Oikopleura longicauda*

Materials and methods

Animals

Oikopleura dioica was collected near the Seto Marine Biological Laboratory on the Kii peninsula, Wakayama, Japan, and cultured in 5-l beakers with constant stirring at 18°C as described previously [9]. To sample juvenile (days 1–3) and adult (days 4–5) stages, animals were transferred to plastic dishes, rinsed with artificial sea water (Rohto-marine, Rei-Sea), and fixed with 4% paraformaldehyde in 0.5 M NaCl, 0.1 M morpholinepropanesulfonic acid (pH 7.5) for 12 h at 4°C. Animals were washed twice with phosphate-buffered saline containing 0.1% Tween 20 (PBS-T), dehydrated in an ethanol series, and stored in 80% ethanol at −20°C. Unless otherwise indicated, all washing steps were performed in PBS-T for 10 min at room temperature. To sample embryonic stages, naturally spawned eggs from a single female were inseminated in seawater containing sperm from one or more males. Fertilized eggs were rinsed in artificial seawater, left to develop at 18°C, and collected at different developmental stages [6] to be fixed as described above. *O. longicauda* was collected near the Misaki Marine Biological Station on the Miura Peninsula, Kanagawa, Japan, and immediately fixed as described above. Pyurid ascidian *Halocynthia roretzi* and molgulid ascidian *Molgula tectiformis* were collected near the International Coastal Research Center on the Bay of Otsuchi, Iwate, Japan.

Immunochemical visualization of possible cellulosic structure

Fixed samples were hydrated, incubated in PBS containing 1% blocking reagent (Roche) for 1 h at room temperature, and incubated, for 12 h at 4°C, in PBS containing 20 mg/ml cellulose binding domain protein from *Clostridium cellulovorans* (Sigma), which is placed in carbohydrate-binding module family 3 in the Carbohydrate Active Enzymes database (http://www.cazy.org/). After five washes, samples were incubated in PBS containing 1% blocking reagent/1 ng/ml anti-cellulose binding domain mouse antisera (Sigma) for 1 h at room temperature. After six washes, samples were incubated in PBS containing 1% blocking reagent/1 ng/ml anti-mouse goat IgG conjugated with Alexafluor 488 (Invitrogen) for 12 h at 4°C. After ten washes, samples were counterstained with 1 ng/ml TO-PRO-3 (Invitrogen) in PBS-T for 20 min at room temperature. After two washes, samples were mounted on slides with Vectashield mounting medium (Invitrogen). Images were acquired under the LSM510 confocal system (Zeiss).

Electron microscopy

Fixed samples were hydrated, mounted on copper grids with a carbon support film (NetMesh Lacey Carbon Type-A, Ted Pella), and rapidly frozen by immersion in liquid ethane with a rapid freezing device (KF80, Reichert). Frozen samples were quickly transferred in a vacuum coating system (Auto 306, Edwards) to be freeze-dried, sputter-coated with platinum, and observed under a high-resolution field emission-scanning electron microscope (JSM-6700F, JEOL). For transmission electron microscopy (TEM), animals were fixed with 2.5% glutaraldehyde, 0.45 M sucrose, 0.1 M cacodylate buffer (pH 7.5) at 4°C for 2 h; briefly rinsed with the same buffer; post-fixed with 1% osmium tetroxide, 0.1 M cacodylate buffer (pH7.5) at 4°C for 1.5 h; dehydrated in an ethanol series; and embedded in an epoxy resin. Sections were stained with uranyl acetate and lead citrate and examined under the transmission electron microscope JEM-1010 (JEOL).

Electron diffraction

Day 4 animals were transferred to plastic dishes, washed with fresh seawater, and left to renew their houses. To avoid contamination, houses were only collected immediately after inflation. Houses were incubated twice in PBS-T containing 0.1 mg/ml proteinase K for 36 h at 42°C. After five washes, samples were rinsed with deionized water and

mounted on a copper grid. Electron diffraction patterns were obtained with the JEM2000-EXII transmission electron microscope (JEOL) under low-dose exposure with the help of a GATAN 622-0600 image intensifier as described previously [10]. Larval samples were assessed without proteinase K treatments.

Fourier transform infrared (FTIR) spectroscopic microscopy

Sample preparations were performed as for electron beam diffraction. Infrared spectra were obtained with AutoIMAGE FTIR microscope system (Perkin Elmer) as described previously [11]. Allomorph compositions were estimated from a calibration curve drawn with algal and tunicate samples whose allomorph ratios have been verified [10, 12].

Molecular cloning

Total RNAs were isolated from tailbud and day 4 specimens of *O. dioica* or adult specimens of *H. roretzi* and *M. tectiformis* by the guanidium thiocyanate-acid phenol method using RNAlater (Ambion) and TRizol reagent (Invitrogen). First-strand cDNA synthesis was done by incubating DNase I (Invitrogen)-treated total RNAs with SuperScript III reverse transcriptase (Invitrogen) and oligo(dT)12–18 primer following the manufacturer's instructions. Degenerate PCR was performed using KOD-Plus-Ver.2 DNA polymerase (Toyobo) and primers designed to match amino acid sequences conserved among known cellulose synthases. Amplicons were subcloned into pCR-Blunt II TOPO vectors using Zero Blunt PCR Cloning kit (Invitrogen) and sequenced with BigDye Terminator sequencing kit (Applied Biosystems). Rapid amplifications of 5′ and 3′ cDNA ends (5′ and 3′ RACE) were performed using gene-specific primers and SMART RACE cDNA amplification kit (Clontech). Genomic DNA was isolated from day 4 specimens of *O. dioica* using a PureLink Genomic DNA kit (Invitrogen). Genomic sequences were PCR amplified, subcloned, and sequenced as described above. We also used cDNA and genomic DNA libraries of *O. longicauda* as PCR templates [13]. The isolated sequences were used as a query for in silico cloning on the open database of Norwegian *O. dioica* at Genoscope (http://www.genoscope.cns.fr/blat-server/cgi-bin/oikopleura/webBlat). Molecular phylogenetic analysis was performed using putative cellulose synthase sequences listed in Data S1 as described previously [14].

Real-time quantitative PCR (qPCR)

RNA isolation and first-strand cDNA synthesis were performed as described above. qPCR was done using Prism 7000 sequence detection system (Applied Biosystems) and Thunderbird qPCR mix (Toyobo) in a reaction volume of 50 µl. The amount of cDNA templates was empirically determined in order to fall in the range of standard curve drawn with control plasmids. After initial denaturation for 1 min at 95°C, 40 cycles of 95°C for 15 s, and 60°C for 30 s were conducted. Ribosomal protein L23 (RbL23) was used as a normalization control. Reaction products were verified by agarose gel electrophoresis, subcloning, and sequencing. Primer sequences and concentrations were as follows: *Od-CesA1* (GACCATATTGTTGACGTGCTTCAG and CTCAGATGCCAGTTGCATATTGTAG; 240 nM), *Od-CesA2* (ACTCCGAAAATCTCCAGGAAGTC and CAACCTGGAACTCAGTGTTATGGT; 220 nM), and *Od-RbL23* (GCCAGAACTCCGAAAGAAGGT and CACCGGCGTTATCTTCGAA; 48 nM).

Whole-mount in situ hybridization

Full-length cDNA fragments encoding *Od-CesA1* or *Od-CesA2* were PCR amplified with primer pairs containing either T3 or T7 promoter sequences. PCR products were column-purified and used as a template for in vitro transcription of sense or antisense RNA probes using T3 or T7 RNA polymerases in the presence of digoxigenin-labeled UTP (Roche). Fixed specimens were hydrated, washed twice, and incubated in PBS-T containing 5 µg/ml proteinase K at 37°C (1 min for larvae, 3 min for juvenile, and 5 min for adult samples). After brief washes, samples were fixed in PBS-T containing 4% paraformaldehyde for 5 min at room temperature. After three washes, samples were incubated in prehybridization solution [50% formamide, 5× standard saline citrate (SSC), 5× Denhardt solution (Nacalai tesque), 1.45 mg/ml yeast tRNA (Invitrogen), 0.1% Triton X-100] for 3 h at 55°C. Samples were hybridized in prehybridization solution containing 50 ng/ml RNA probe for 16 h at 53°C. Samples were washed twice in 50% formamide, 5× SSC, 0.1% Triton X-100 for 15 min at 37°C; twice in 50% formamide, 2× SSC, 0.1% Triton X-100 for 15 min at 37°C; and twice in 0.5× SSC, 1% blocking reagent, 0.1% Triton X-100 for 15 min at 55°C. After two washes in NTE solution (500 mM NaCl, 10 mM Tris-HCl, 1 mM EDTA) for 10 min at room temperature, samples were incubated in NTE solution containing 20 µg/ml RNase A (Invitrogen) for 30 min at 37°C. After four washes, samples were incubated in blocking solution [PBS-T/10% blocking reagent/5% sheep serum (Funakoshi)] for 1 h at room temperature, followed by incubation in blocking solution containing 1 ng/ml anti-digoxigenin sheep Fab fragments conjugated with alkaline phosphatase (Roche) for 12 h at 4°C. After ten washes, samples were washed three times in 0.1 M Tris-HCl (pH 8.0), 0.1 M NaCl, 50 mM $MgCl_2$ for 10 min at room

temperature. Signal detection was carried out using nitroblue tetrazolium and 5-bromo-4-chloro-3-indolyl phosphate stock solutions (Roche).

Results and discussion

We performed whole-mount fluorescent immunohistochemistry using carbohydrate binding module protein (CBM) [15] as a probe, and this enabled the visualization of possible cellulosic structures: the house, scale-like structures, and larval body cuticle (Fig. 1e–t). Rudimentary houses consisted of extracellular matrices covering the anterior trunk epidermis, and tail beating inflates the houses allowing them to attain their functional state (Fig. 1e–g). House inflation took less than 1 min, and the structural framework of a tertiary house likely arises inside the rudiments during secretion by epidermal cells lining the rudiments through unknown mechanisms. The house-secreting cells, which have a large nucleus due to endoreduplications [16], were arranged in a species-specific bilateral pattern that corresponds to the structural organization of house rudiments (Fig. 1h) [17]. The remaining portion of the epidermis that covers the posterior trunk and the tail consisted of hexagonal flat cells that were stained with CBM (Fig. 1i, j). Alkaline treatment of intact organisms generated an exoskeleton-like capsule consisting of hexagonal scale-like structures, which were confirmed to be an intracellular deposition by TEM (Fig. 1k–m). Subsequent acid hydrolysis revealed a monolayer of fine meshwork embedded in an unknown matrix, and this meshwork accounted for the observed CBM signals (Fig. 1n, o). The larval epidermis, not yet differentiated into the two cell types of the adult stage, is enclosed by a thin cuticle [6, 18], which was stained with CBM (Fig. 1p, q). The cuticle formed fins on the dorsal and ventral midlines of the tail, and it was contiguous with the prominent caudal fin that contains many fibrils extending posteriorly as observed by FE-SEM and TEM (Fig. 1r–t). A rudimentary caudal fin was detectable in the embryo. It became elongated after hatching and was lost in a metamorphic moult prior to the secretion of the first house rudiment.

The CBM used as a probe in these experiments is capable of binding polysaccharides other than cellulose including chitin [19], so we confirmed that cellulose occurs in the examined structures using electron diffraction. The diffractogram obtained from a purified house was of typical tunicate cellulose: an almost pure I_β allomorph [20], as identified with 002 spots [7, 10, 21] (Fig. 2a, b). In contrast, 002 spots were absent from the diffractogram of a caudal fin, wherein almost all diffraction spots were indexed with the triclinic unit cell of I_α allomorph, as exemplified by $\bar{1}03$ spots [10, 21] (Fig. 2c, d). The scale-like structures were too thick to allow for assessment. We confirmed these results by FTIR microscopy designed for tiny samples [11]. The spectrum obtained from a purified house contained an absorbance peak specific to I_β allomorph at 3,270 cm^{-1}, and the spectrum from a caudal fin contained a I_α-specific peak at 3,240 cm^{-1} [22] (Fig. 2e). The peak assigned to intrachain hydrogen bonding between O5-H-O3 showed a spectral shift around 3,340–3,450 cm^{-1} [23], and this linearly correlated with the I_α allormorph composition (Fig. 2f). The estimated I_α fraction was about 3% for a purified house versus 93% for a caudal fin, which is among the highest in nature [12]. Given that allomorph ratios of native cellulose are species-dependent and constant, the radical change in the allomorph ratio seen over the course of the life cycle of *Oikopleura* is unusual.

To better understand the molecular mechanisms underlying the formation of different allomorphs, we isolated and characterized putative *O. dioica* homologs of the cellulose synthase gene (*CesA*) that is the catalytic subunit of the cellulose-synthesizing membrane protein complexes termed terminal complexes (TCs) [24, 25]. The genomes of two ascidian species have been sequenced, and they contain a single *CesA* locus [14, 26]. However, our degenerate PCR-based isolation identified two isoforms: *Od-CesA1*, encoding 1,257 amino acid residues in nine exons, and *Od-CesA2*, encoding 1,251 amino acid residues in ten exons (Fig. 3a, Fig. S1). These two proteins, exhibiting 68% amino acid identity, contain molecular signatures that are common to glycosyl transferase family 2 (GT2) members or specific to CesA subfamily members [14] (Fig. S1). We examined their spatiotemporal expression patterns by quantitative real-time PCR (qPCR) and in situ hybridization (Fig. 3b–m). Expression signals of *Od-CesA1* were conspicuous all over the epidermis in late embryonic stages (Fig. 3c), confined to the posterior trunk epidermis after hatching (Fig. 3d, e), and almost ceased in juvenile and adult stages (Fig. 3f). In contrast, expression signals of *Od-CesA2* were faint before hatching (Fig. 3g), but strong signals were seen in late larval, juvenile, and adult stages, forming bilateral patterns on the anterior trunk epidermis (Fig. 3h–m). We observed a variety of bilateral patterns of *Od-CesA2* expression, which might represent snapshots of different phases of cyclic genetic programs underlying the repetitive process of house reproductions. Collectively, the mutually exclusive expression patterns of the two *O. dioica CesA* homologs spatiotemporally correspond to the secretion sites of two cellulosic structures made of different allomorphs.

The *Od-CesA*s encode a fusion protein of a CesA domain and a cellulase domain of glycosyl hydrolase family 6 (GH6). Cellulase is important for cellulose biosynthesis in bacteria and plants [27], but a fusion gene containing *CesA* and cellulase is unique to tunicate homologs including three

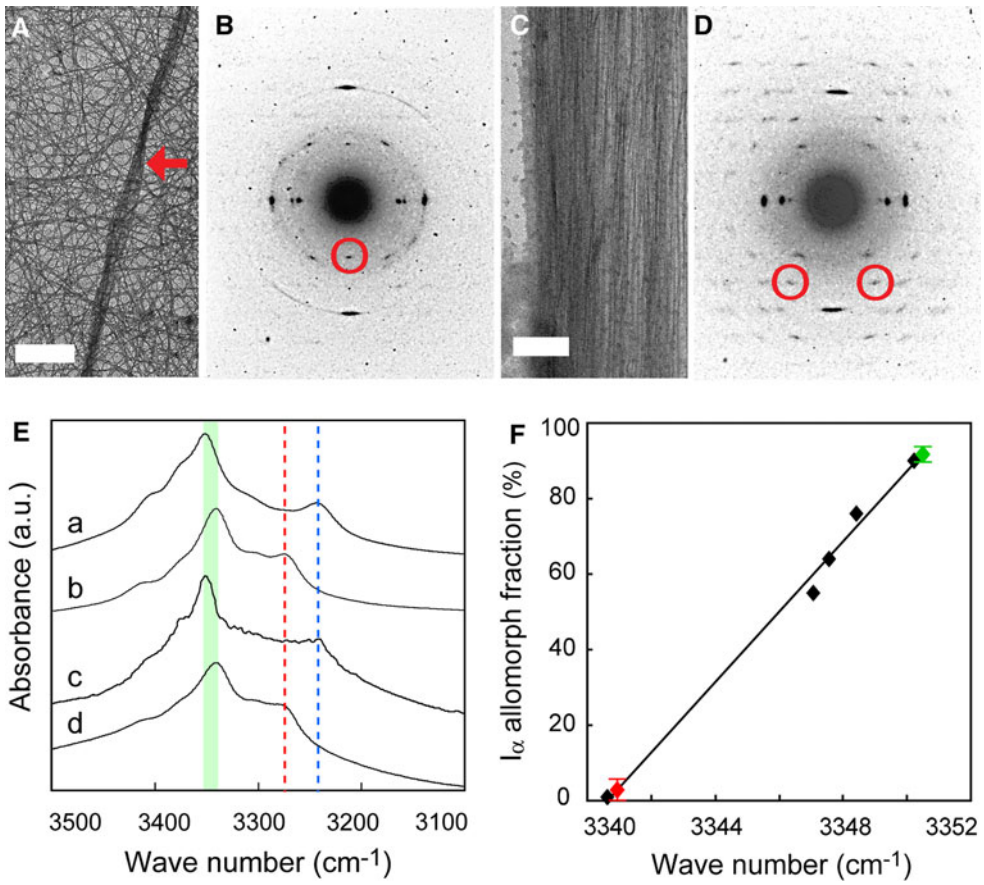

Fig. 2a–f Characterization of *Oikopleura* cellulose. **a**–**d** Electron diffraction. **a** A bright-field diffraction contrast image of a purified house shows single fibers in a random orientation and some bundled fibers (*red arrow*). **b** The electron diffraction diagram of a purified house demonstrates a meridional 002 monoclinic spot indicated with a *red circle*. **c** A bright-field diffraction contrast image of a caudal fin shows anteroposteriorly aligned fibers. **d** The electron diffraction diagram of a caudal fin demonstrates diffraction spots up to 6th layer lines, showing the highly ordered crystalline nature of cellulose microfibrils. Two $\bar{1}03$ triclinic spots are indicated with *red circles*. **e**, **f** FTIR microscopy. **e** FTIR spectra of I_α-rich cellulose (*a* glaucophyte *Glaucocystis nostochinearum*), I_β-rich cellulose (*b* ascidian *Halocynthia roretzi*), caudal fin (*c*), and purified house (*d*) are shown. Allomorph-specific band positions are indicated with *blue* (I_α) and *red* (I_β) *lines*. Spectral shifts of the peak assigned to intrachain hydrogen bondings between O5-H-O3 are featured (*green*). **f** There was a linear correlation between the spectral shift and allomorph composition ($R^2 = 0.99$). I_α fractions of standards are as follows: *H. roretzi*, 0.01; chlorophyte *Boergesenia forbesii*, 0.55; chlorophyte *Valonia ventricosa*, 0.64; chlorophyte *Cladophora* sp., 0.76; and *G. nostochinearum*, 0.90. *Oikopleura* samples are featured in *red* (purified house) and *green* (caudal fin). *Error bars*, s.d., $n = 8$

and two newly isolated appendicularian and ascidian homologs, respectively (Fig. S1). Based on this fusion, it has been argued that the horizontal transfer of a bacterial *CesA* gene might have contributed to the establishment of cellulose biosynthesis in tunicates, the only animals capable of cellulose biosynthesis [14, 26]. Molecular phylogenetic analyses of either CesA or GH6 suggest monophyly of tunicate homologs, within which appendicularian and ascidian homologs form independent clades (Fig. 4a–b; Fig. S2A, B). These data support a single origin for tunicate homologs and subsequent gene duplication in the appendicularian lineage. Duplicated genes successfully maintained in genomes typically evolve distinct functions [28], and it remains unclear if this is true for different allomorphs found in *Oikopleura* cellulose. The ability of appendicularians to synthesize I_α allomorph likely arose from a pre-existing ability to synthesize I_β allomorph, given that the dominant allomorph of tunicate cellulose is I_β. Alternatively, the various cellulosic structures of tunicates might be explained in the context of parallel evolution [29], wherein an ancestral ability to synthesize cellulose in the tunicate progenitor was subjected to lineage-specific modifications to form independent structures (Fig. 4c).

Native cellulose forms a hierarchical structure in which β-1,4-glucan chains are organized into crystalline fibrillar composites, with structural variations at any level of organization, e.g., fibril shape, crystalline size, or crystalline phase, all of which influence the physicochemical properties of the whole structure [30]. Differences between triclinic and monoclinic units can be attributed to distinct

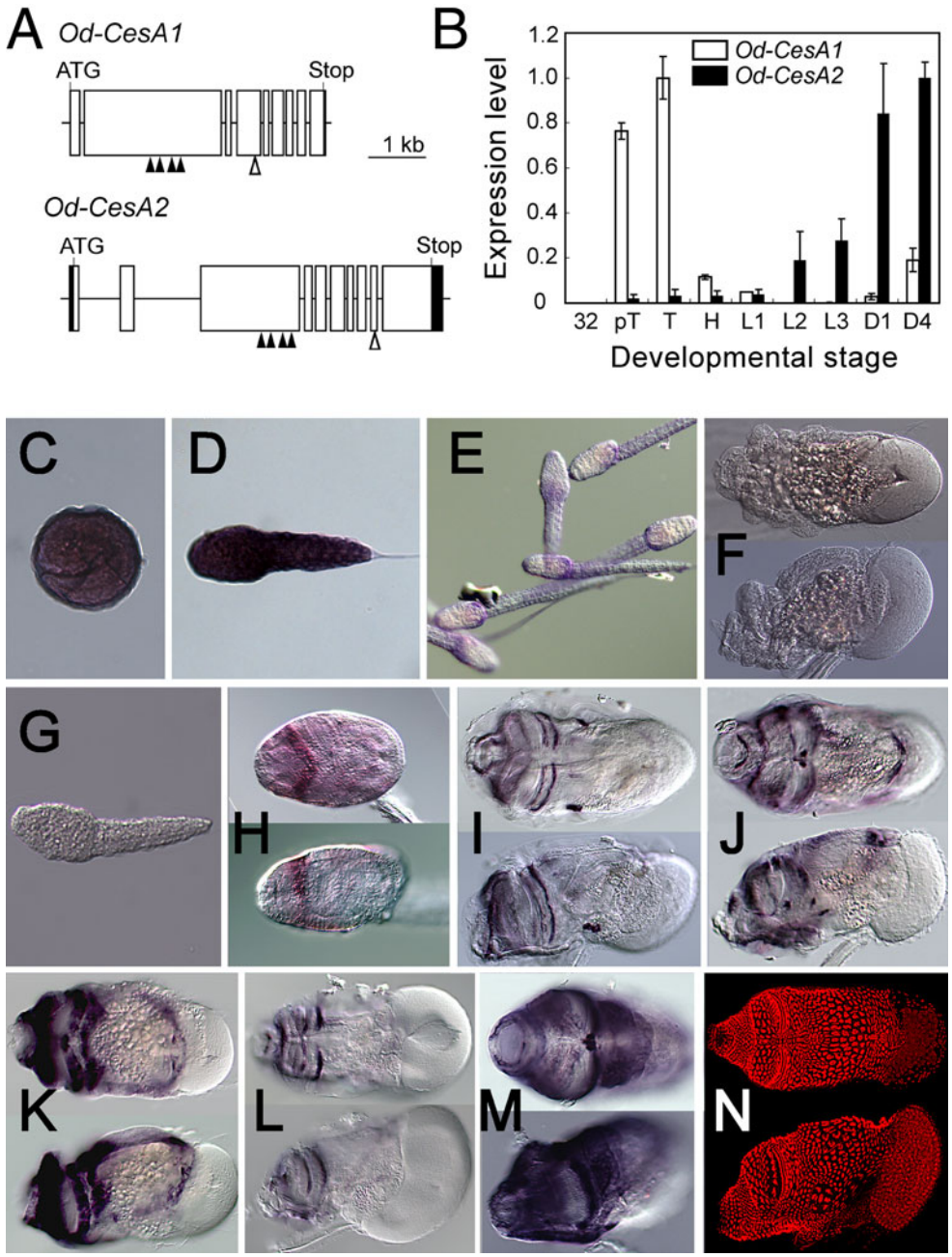

Fig. 3a–n Putative cellulose synthase genes of *Oikopleura dioica*. **a** Intron-exon structures of *Od-CesA1* and *Od-CesA2*. *Open box* indicates the coding region of exon, the *shaded box* the noncoding region of exon, *bar* intron, *ATG* putative start codon of ORF, *Stop* stop codon of ORF, *shaded triangle* molecular signature of glycosyl transferase family 2, i.e., the D-DxD-D-QxxRW motifs, *open triangle* molecular signature of glycosyl hydrolase family 6 [PROSITE accession number: PS00656 (http://kr.expasy.org/prosite/)]. Detailed characterizations are given in Fig. S1. **b**—**n** *Od-CesA1* and *Od-CesA2* are differentially expressed. **b** Real-time quantitative PCR expression profiles are shown. Expression levels are relative to the highest value, TB for *Od-CesA1* and Day 4 for *Od-CesA2*. PCR amplifications were verified to be cDNA-derived, except *Od-CesA1* at Day 4 where amplifications are due to genomic contamination. Developmental stages are as follows: *32* 32 cell embryo, *pT* pre-tailbud embryo, *T* tailbud embryo, *H* hatched larva, *L1* larval stage 1, *L2* larval stage 2, *L3* larval stage 3, *D1* 1 day post fertilization adult, *D4* 4 days post fertilization adult. *Error bars* indicate s.d., $n = 4$. **c–f** In situ hybridization profiles of *Od-CesA1* are shown. **c** Tailbud embryo. **d** Hatched larva. **e** Larval stage 3. **f** Day 4 adult (*upper panel* dorsal view, *lower panel* lateral view). **g–m** In situ hybridization profiles of *Od-CesA2*. **g** Hatched larva. **h** Larval stage 3. **i–m** Day 4 adults (*upper panel* dorsal view, *lower panel* lateral view). Note that these patterns correspond to distinct portions of the house-secreting epithelium of *O. dioica*. **n** Nuclear staining with TO-PRO-3

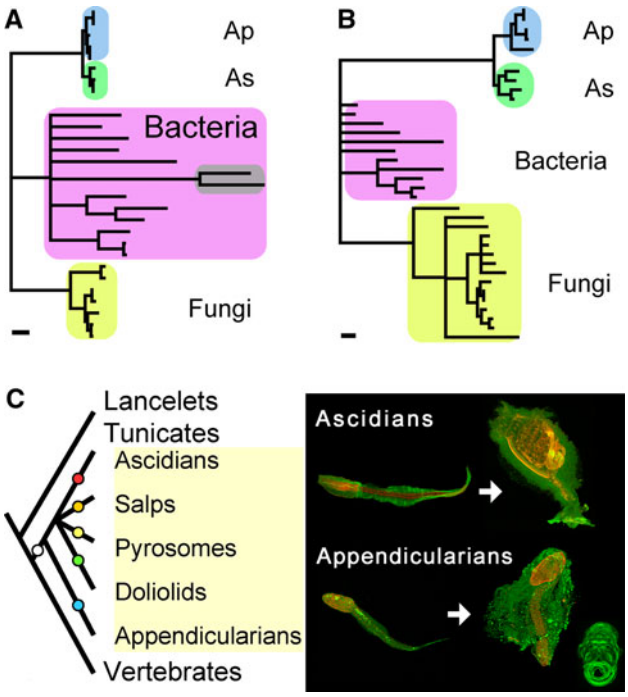

Fig. 4a–c Tunicate phylogeny in light of cellulose biosynthesis. **a**−**b** Molecular phylogeny of tunicate cellulose synthases. **a** The most likely tree for the putative cellulose synthase domain, inferred using a quartet maximum-likelihood method (log likelihood = −4,887.83, 166 amino acid sites). The original version is shown in Fig. S2A. The percent support for monophyletic tunicates, ascidians (*As*), and appendicularians (*Ap*) are, respectively, 98, 85, and 68% (quartet puzzling support values in quartet maximum-likelihood method) or 100, 86, and 62% (bootstrap values in neighbor-joining method). The cyanobacterial clade to which plant sequences form a sister clade, if included in the analysis [14, 35], are featured in *gray*. The *scale bar* represents 0.1 substitutions per site. **b** The most likely tree for the glycosyl hydrolase family 6 domain, inferred using a quartet maximum-likelihood method (log likelihood = −4,274.04, 110 amino acid sites). The original version is shown in Fig. S2B. The percent support for monophyletic tunicates, ascidians (*As*), and appendicularians (*Ap*) are, respectively, 96, 88, and 97% (quartet puzzling support values in quartet maximum-likelihood method) or 100, 85, and 76% (bootstrap values in neighbor-joining method). The *scale bar* represents 0.1 substitutions per site. **c** Parallel evolution of cellulose biosynthesis in tunicates. Tunicates are invertebrate chordates and a sister group of vertebrates (*left*). The inferred monophyly of tunicate CesAs supports the single origin of cellulose biosynthesis within the tunicate lineage (*white circle*). Various cellulosic structures with their own morphology and function may be products of lineage-specific modifications (*colored circles*), as suggested by our study (*right*). Both larval ascidians and appendicularians retained the common tadpole-like chordate body plan with contiguous median and caudal fins [36]. Only larval appendicularians possess the ability to synthesize I_α allomorph. Adult ascidians generate various cellulosic structures [37] and possess migratory cells specialized for the maintenance of the cellulosic protective coat, which is indispensable for their sessile life style [38]. Adult appendicularians possess a filter-feeding house and its requisites: adult tail, house-secreting epithelium, and cyclic expressions of *CesA*

arrangements of 0.39-nm lattice planes along the *c*-axis [21], which molecular simulations suggest are settled in van der Waals–associated glucan sheets at the very onset of crystallization under stereochemical constriction placed by TCs [31–33]. Consequently, the coincidence between different allomorphs and different isoforms of the catalytic subunit of TCs might represent a possible link between structural variations in the crystalline phases and underlying genetic processes leading to their synthesis. This should be tested in future studies. Our current knowledge is largely derived from studies motivated by industrial demands for controlling the properties of biosynthetic materials, and structural variations are considered unfavorable factors in manufacturing quality control. However, we now appreciate that a new biological function is achieved when different microstructures of cellulose crystals are organized into a single structure [34]. Therefore, structural variations might, at least in part, reflect functional adaptations of cellulose crystals. The minor animal model *Oikopleura* may contribute to our understanding of how structural variations in cellulose crystals can be explained in a biological context.

Acknowledgments We thank Dr. Tomoya Imai for valuable discussion, Dr. Yutaka Satou for the qPCR facility, Prof. Hiroyuki Yano for the FE-SEM facility, Dr. Fuki Gyoja for sampling *Molgula tectiformis*, and staff members of the Misaki Marine Biological Station, University of Tokyo, and Seto Marine Biological Station, Kyoto University, for sampling *Oikopleura longicauda* and *Oikopleura dioica*, respectively. The nucleotide sequences for the reported genes have been deposited with the GenBank under accession codes AB543594 (*Od-CesA1*) and AB543593 (*Od-CesA2*). K.N. designed research, performed experiments, and wrote the manuscript. A.N. performed collection, culture, and preparation of appendicularians. Y.H. and J.S. performed electron diffraction and FTIR microscopy. E.H. performed transmission electron microscopy. N.S. supervised reseach. All authors discussed the results and commented on the manuscript. The authors declare no competing financial interests. This work was supported by Grants-in-Aid for Young Scientists to K.N. (no. 18770046 and 21780166) and Grant-in-Aid to N.S. (no. 17018018) from the Ministry of Education, Culture, Sports, Science and Technology (MEXT) of Japan. This work was also partly supported by Intellectual Cluster Formation of Okinawa Prefecture, Japan.

References

1. Flood PR (1991) Architecture of, and water circulation and flow-rate in, the house of the planktonic tunicate *Oikopleura labradoriensis*. Mar Biol 111:95–111
2. Gorsky G, Fenaux R (1998) The role of Appendicularia in marine food webs. In: Bone Q (ed) The biology of pelagic tunicates. Oxford University Press, New York
3. Sato R, Tanaka Y, Ishimaru T (2003) Species-specific house productivity of appendicularians. Mar Ecol Prog Ser 259:163–172
4. Alldredge A (2005) The contribution of discarded appendicularian houses to the flux of particulate organic carbon from oceanic surface waters. In: Gorsky G, Youngbluth MJ, Deibel D (eds) Response of marine ecosystems to global change: ecological impact of Appendicularians. Editions Scientifiques GB, Paris

5. Nielsen C (2001) Animal evolution: interrelationships of the living phyla. Oxford University Press, New York
6. Fenaux R (1998) Life history of the appendicularia. In: Bone Q (ed) The biology of pelagic tunicates. Oxford University Press, New York
7. Kimura S, Ohshima C, Hirose E, Nishikawa J, Itoh T (2001) Cellulose in the house of the appendicularian *Oikopleura rufescens*. Protoplasma 216:71–74
8. Shubin N, Tabin C, Carroll S (2009) Deep homology and the origins of evolutionary novelty. Nature 457:818–823
9. Fujii S, Nishio T, Nishida H (2008) Cleavage pattern, gastrulation, and neurulation in the appendicularian, *Oikopleura dioica*. Dev Genes Evol 218:69–79
10. Imai T, Sugiyama J (1998) Nanodomains of I_α and I_β cellulose in algal microfibrils. Macromolecules 31:6275–6279
11. Nakashima K, Sugiyama J, Satoh N (2008) A spectroscopic assessment of cellulose and the molecular mechanisms of cellulose biosynthesis in the ascidian *Ciona intestinalis*. Mar Genomics 1:9–14
12. Imai T, Sugiyama J, Itoh T, Horii F (1999) Almost pure I_α cellulose in the cell wall of *Glaucocystis*. J Struct Biol 127:248–257
13. Nishino A, Satou Y, Morisawa M, Satoh N (2001) *Brachyury (T)* gene expression and notochord development in *Oikopleura longicauda* (Appendicularia, Urochordata). Dev Genes Evol 211:219–231
14. Nakashima K, Yamada L, Satou Y, Azuma J, Satoh N (2004) The evolutionary origin of animal cellulose synthase. Dev Genes Evol 214:81–88
15. Boraston AB, Bolam DN, Gilbert HJ, Davies GJ (2004) Carbohydrate-binding modules: fine-tuning polysaccharide recognition. Biochem J 382:769–781
16. Ganot P, Thompson EM (2002) Patterning through differential endoreduplication in epithelial organogenesis of the chordate, *Oikopleura dioica*. Dev Biol 252:59–71
17. Flood PR (2005) Toward a photographic atlas on special taxonomic characters of oikopleurid Appendicularia (Tunicata). In: Gorsky G, Youngbluth MJ, Deibel D (eds) Response of marine ecosystems to global change: ecological impact of Appendicularians. Editions Scientifiques GB, Paris
18. Stach T (2007) Ontogeny of the appendicularian *Oikopleura dioica* (Tunicata, Chordata) reveals characters similar to ascidian larvae with sessile adults. Zoomorphology 126:203–214
19. Goldstein MA, Takagi M, Hashida S, Shoseyov O, Doi RH, Segel IH (1993) Characterization of the cellulose-binding domain of the *Clostridium cellulovorans* cellulose-binding protein A. J Bacteriol 175:5762–5768
20. Belton PS, Tanner SF, Cartier N, Chanzy H (1989) High-resolution solid-state ^{13}C nuclear magnetic resonance spectroscopy of tunicin, an animal cellulose. Macromolecules 22:1615–1617
21. Sugiyama J, Vuong R, Chanzy H (1991) Electron diffraction study on the two crystalline phases occurring in native cellulose from an algal cell wall. Macromolecules 24:4168–4175
22. Sugiyama J, Persson J, Chanzy H (1991) Combined infrared and electron diffraction study of the polymorphism of native celluloses. Macromolecules 24:2461–2466
23. Marechal Y, Chanzy H (2000) The hydrogen bond network in I_β cellulose as observed by infrared spectrometry. J Mol Struct 523:183–196
24. Guerriero G, Fugelstad J, Bulone V (2010) What do we really know about cellulose biosynthesis in higher plants? J Integr Plant Biol 52:161–175
25. Joshi CP, Mansfield SD (2007) The cellulose paradox-simple molecule, complex biosynthesis. Curr Opin Plant Biol 10:220–226
26. Matthysse AG, Deschet K, Williams M, Marry M, White AR, Smith WC (2004) A functional cellulose synthase from ascidian epidermis. Proc Natl Acad Sci USA 101:986–991
27. Mølhøj M, Pagant S, Höfte H (2002) Towards understanding the role of membrane-bound endo-beta-1,4-glucanases in cellulose biosynthesis. Plant Cell Physiol 43:1399–1406
28. Conant GC, Wolfe KH (2008) Turning a hobby into a job: how duplicated genes find new functions. Nat Rev Genet 9:938–950
29. Gould SJ (2002) The structure of evolutionary theory. Harvard University Press, Cambridge
30. Nishiyama Y (2009) Structure and properties of the cellulose microfibril. J Wood Sci 55:241–249
31. Cousins SK, Brown RM (1995) Cellulose I microfibril assembly: computational molecular mechanics energy analysis favours bonding by van der Waals forces as the initial step in crystallization. Polymer 36:3885–3888
32. Cousins SK, Brown RM (1997) X-ray diffraction and ultrastructural analyses of dye-altered celluloses support van der Waals forces as the initial step in cellulose crystallization. Polymer 38:896–902
33. Cousins SK, Brown RM (1997) Photoisomerization of a dye-altered β-1,4 glucan sheet induces the crystallization of a cellulose-composite. Polymer 38:903–912
34. Elbaum R, Zaltzman L, Burgert I, Fratzl P (2007) The role of wheat awns in the seed dispersal unit. Science 316:884–886
35. Nobles DR, Brown RM (2007) Many paths up the mountain: tracking the evolution of cellulose biosynthesis. In: Brown RM, Saxena IM (eds) Cellulose: molecular and structural biology. Springer, Dordrecht
36. Pasini A, Amiel A, Rothbacher U, Roure A, Lemaire P, Darras S (2006) Formation of the ascidian epidermal sensory neurons: insights into the origin of the chordate peripheral nervous system. PLoS Biol 4:1173–1186
37. Kimura S, Itoh T (2007) Biogenesis and function of cellulose in tunicates. In: Brown RM, Saxena IM (eds) Cellulose: molecular and structural biology. Springer, Dordrecht
38. Hirose E (2009) Ascidian tunic cells: morphology and functional diversity of free cells outside the epidermis. Invertebr Biol 128:83–96